Specific Millimeter-Wave Features of Fabry-Perot Resonator for Spectroscopic Measurements

Petr Piksa, Stanislav Zvánovec and, Petr Černý
Czech Technical University in Prague
Czech Republic

1. Introduction

The spectral resolution and intensity sensitivity represent crucial quality parameters for millimeter-wave spectroscopic measurements. A Fabry-Perot resonator (see Fig. 1) can, very efficiently, enhance the sensitivity of the absorption as well as of emission measurements in the millimeter-wave spectroscopy (Zvanovec et al., 2009) (Grabow, 2009). For the monochromatic radiation, the resonator can be tuned to a resonance at which the constructive interference of the multiple-reflected electromagnetic waves enables to accumulate the radiated energy. The higher sensitivity to weak absorptions (resulting from the apparent lengthening of the optical path length by means of multiple reflections) stands for the main advantage of the Fabry-Perot resonator.

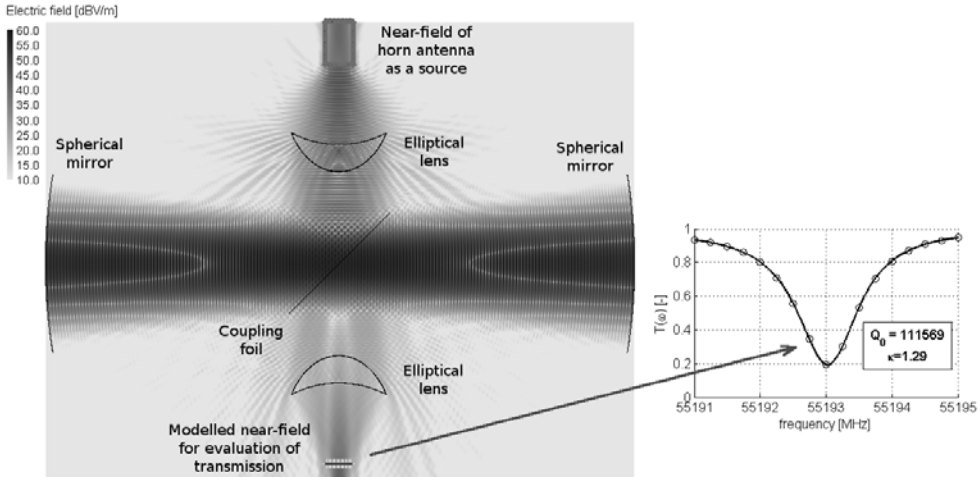

Fig. 1. Model of Fabry-Perot resonator with electric field distribution and enumerated quality factor from resonance curve

This chapter deals with the millimeter-wave features of the Fabry-Perot resonator as a tool for spectroscopic measurements. These features derived from the theoretical knowledge were investigated by means of the results of full-wave numerical modeling in connection with Multi Level Fast Multipole Method (MLFMM) (Chew et al., 2001) and Uniform Theory of Diffraction (UTD) approximation of Method of Moments (MoM). Firstly, the theoretical solution is introduced and then the development and comparison of several models of Fabry-Perot resonator (see an example in Fig. 1) are subject to in-depth analysis and discussion. A simplified model able to solve the resonator performance up to 110 GHz (the radius of the mirrors equals 55 times the wavelength) is introduced. Simulation aspects of specific parts of measuring system are investigated as well. Based on the aforementioned investigations, the full model is proposed.
Last but not least, the attention is paid to the description of the unified technique for obtaining a spectrum of absorption coefficient from the measured resonance curves of the gas-filled as well as evacuated resonators.

2. Fabry-Perot resonator

The majority of Fabry-Perot resonators, when applied to the millimeter-wave spectrum, provide a suited tool to making sensitive and accurate medium loss and dispersal measurements.
Types of Fabry-Perot arrangements, which are usually used, range with respect to the excitation and coupling of the resonator. Either axial or radial excitations of resonator cavity are possible. The resonator can be connected either for measurement of transmission through the resonator or for measurement of reflection by the resonator with the corresponding coupling. The radial excitation utilizes a coupling through a thin dielectric foil (French & Arnold, 1967), where it is possible to excite the dominant mode TEM_{00} without any additional higher-order modes. On the other hand, the dielectric coupling foil decreases a quality factor of the resonator. The axial excitation is realized either by waveguides and coupling holes (Zimmerer, 1963) (Hirvonen et al., 1996), or by coaxial lines and inductive coupling or an L-shaped antenna (Montgomery, 1947, p. 318) (Grabow, 2009, p. 423).
The investigated Fabry-Perot resonator comprises a radial excitation and comprises two spherical mirrors, dielectric coupling foil placed between these mirrors and dielectric lenses necessary for the establishment of the plane wave into/out of the resonator via the coupling foil; see Fig. 1. The radiated energy is coupled into/out of the resonator cavity by means of the special elliptical dielectric lenses (Milligan, 2005, p. 448) (Johnson, 1993, p. 16-4) that are placed in the windows. Moreover, the above-mentioned energy is coupled also via the dielectric polyethylene coupling foil from/to the perpendicularly placed feeder and detector (horn antennas). The lenses focus the required radiated energy on/from the coupling foil and thus form the diverging waveforms in the near field region onto the flat uniform field. The optimization of lenses parameters was accomplished in order to optimize the waveform inside the resonator. It was necessary to avoid additional undesirable resonances inside the resonator that are caused by inner surfaces of lenses, for these resonances evoke a dummy increase of the quality factor. The optimal field distribution on the coupling foil together with the position of the feeding antenna in front of the lens were also carefully sought (Zvanovec et al., 2009).

It is essential to note that the polarization of incident wave in case of the radial excitation affects the coupling into the resonator. The parallel polarization proves a low reflection from the dielectric foil, therefore, the resonator is coupled to a very low extent. Hence solely the perpendicular polarization was utilized.

2.1 Resonance condition

The resonator has to fulfill the following resonance condition:

$$\frac{2d}{\lambda} = q + (2p + l + 1)\frac{1}{\pi}\arccos\left(\sqrt{\left(1 - \frac{d}{R_1}\right)\left(1 - \frac{d}{R_2}\right)}\right) - \frac{1.655t\left(\sqrt{\varepsilon_r} - 1\right)}{\lambda_0 / 2}, \quad (1)$$

where p, l, q are indexes of TEM modes, q means the number of half-wavelengths on the distance d between the mirrors, $R_{1,2}$ stand for the radii of the curvature of mirrors, t is thickness and ε_r is relative permittivity of the dielectric coupling foil. The second part on the right side of (1) introduces the correction from the plane to the spherical wave and the last part of (1) counts for an approximate correction of the dielectric foil.

2.2 Equivalent circuit, coupling coefficient and quality factor

As it has been already mentioned, the investigated resonator is straight-through and the coupling is realized with the thin dielectric foil. The level of the transmitted power therefore depends on the value of the coupling coefficient, quality factor and relative frequency misalignment of the resonator. In the resonance, the transmitted power shows minimum value. Out of the resonance and under the low coupling, the transmitted power is not influenced by the resonator. Thus, the resonator can be described by an equivalent circuit such as the one depicted in Fig. 2b).

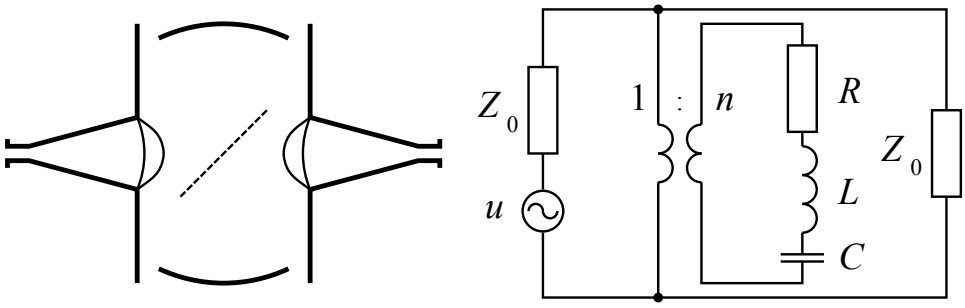

a) b)

Fig. 2. a) Fabry-Perot resonator scheme and b) equivalent circuit

The theoretical solution of the equivalent circuits is based upon the techniques such as (Montgomery, 1947, p. 314). As a result, we can specify the most important parameters of this resonator.

The unloaded quality factor can be defined by equation that follows

$$Q_0 = \frac{\omega_0 L}{R}, \tag{2}$$

where ω_0 is the angular frequency equal to $2\pi f_0$ (f_0 represents the resonant frequency), while the parameters L,R are obvious from Fig. 2b).

The external quality factor, which considers the losses in external feeding lines, can be expressed as

$$Q_V = \frac{\omega_0 L}{\frac{n^2 Z_0}{2}}. \tag{3}$$

The loaded quality factor involving the external and internal losses, can be determined from

$$Q_Z = \frac{\omega_0 L}{R + \frac{n^2 Z_0}{2}}. \tag{4}$$

The relation between the unloaded and loaded quality factor is given by

$$Q_Z = \frac{Q_0}{1+\kappa}, \tag{5}$$

where κ stands for the coupling coefficient defined as

$$\kappa = \frac{Q_0}{Q_V} = \frac{n^2 Z_0}{2R}. \tag{6}$$

Since $1/LC=\omega_0^2$, the impedance of resonance circuit Z_r is modified into the following form

$$Z_r = R\left(1 + \mathrm{j}\frac{\omega_0 L}{R}\left(\frac{\omega}{\omega_0} - \frac{\omega_0}{\omega}\right)\right), \tag{7}$$

where the form in inner brackets equals a double relative frequency misalignment δ within the condition of $\omega \approx \omega_0$; see below

$$\frac{\omega}{\omega_0} - \frac{\omega_0}{\omega} \approx 2\frac{\omega - \omega_0}{\omega_0} = 2\delta. \tag{8}$$

The impedance of the resonance circuit transformed through the transformer (1:n) is under consideration of equations (2), (6) and (8). Thus it can be stated

$$Z_m = \frac{R}{n^2}\left(1 + \mathrm{j}2Q_0\delta\right) = \frac{Z_0}{2\kappa}\left(1 + \mathrm{j}2Q_0\delta\right). \tag{9}$$

Output power P_z on the load Z_0 is determined as

$$P_Z = \frac{1}{8}\frac{|u|^2}{Z_0}\frac{1 + (2Q_0\delta)^2}{(\kappa+1)^2 + (2Q_0\delta)^2}. \tag{10}$$

With respect to the equations listed above, the transmission coefficient $T(\omega)$, given by the output power divided by the maximum output power (at κ=0 and δ=0), is defined as

$$T(\omega) = \frac{1 + (2Q_0\delta)^2}{(\kappa + 1)^2 + (2Q_0\delta)^2} \ . \tag{11}$$

At the resonant frequency (δ=0), the coupling coefficient can be defined as

$$\kappa = \frac{1}{\sqrt{T(\omega_0)}} - 1 \ . \tag{12}$$

In regard of the values of the relative frequency misalignment $\delta_{1,2}$ fulfilling the condition:

$$2Q_0\delta_{1,2} = \pm 1 \ , \tag{13}$$

the unloaded quality factor is determined in the way listed below

$$Q_0 = \frac{1}{\delta_1 - \delta_2} = \frac{f_0}{f_1 - f_2} \ , \tag{14}$$

where frequencies f_1 and f_2 correspond to the relative frequency misalignments $\delta_{1,2}$ from the resonance frequency f_0 and the transmission coefficient at the frequencies $f_{1,2}$ is equal to

$$T(\omega_{1,2}) = \frac{2}{(\kappa + 1)^2 + 1} \ . \tag{15}$$

From the above-explained procedure, we can obtain the resonance curve described as a frequency dependence of the transmission coefficient. Owing to the equation (12), we can obtain the coupling coefficient. Equation (15) serves as a tool for obtaining the values of the tracing transmission coefficient $T(\omega_{1,2})$, whereby we can indicate the frequencies $f_{1,2}$ on the resonance curve. The unloaded quality factor can also be evaluated with the help of the equation (14).

2.3 Losses in Fabry-Perot resonator

It is apparent that there are several types of unwanted losses within the Fabry-Perot resonator that influence the unloaded quality factor. Indeed they call for a very careful attention and treatment. Except for the measured attenuation of an inserted medium, we can distinguish among the diffraction and reflection losses at the mirrors and the coupling losses caused by the dielectric foil.

The diffraction losses α_D are interpolated by the approximation (Zimmerer, 1963) (Engstova, 1973) given by

$$\alpha_D = 29 \cdot 10^{-4.83N'} \ , \tag{16}$$

where

$$N' = \frac{a^2}{\lambda d}\sqrt{1-g} = N\sqrt{1-g} \ , \tag{17}$$

a is the radius of mirrors, N stands for the Fresnel number and g=1-d/R_i, where parameter d represents the distance between the mirrors and R_i radius of curvature of mirrors (R_i=R_1=R_2).

Although simplified expressions of diffraction losses have been published in (Arora and Mongia, 1992), they are inconsistent with the numerical results given by (Fox and Li, 1961). The numerical results and approximation curves of diffraction losses α_D are depicted in Fig. 3.

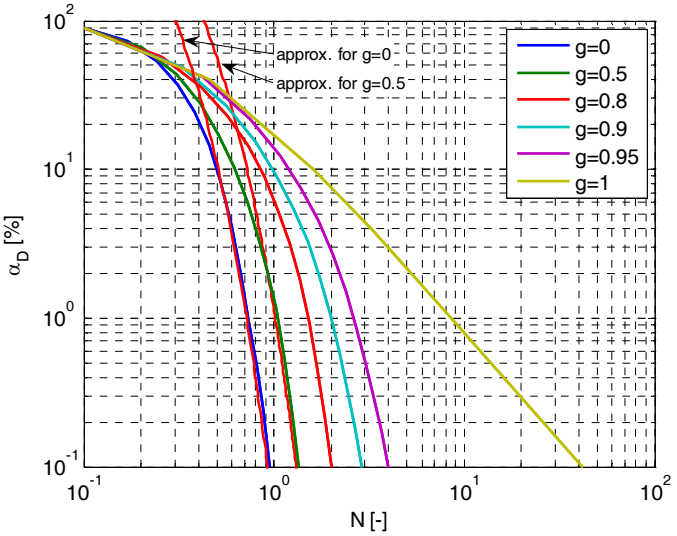

Fig. 3. Coefficient of diffraction losses α_D in dependence on Fresnel number N with approximations given by equation (16)

Reflection losses can be expressed by

$$\alpha_R = 1 - |\rho|^2 \cong 2\sqrt{\frac{2\omega\varepsilon_0\varepsilon_r}{\sigma}} \quad , \tag{18}$$

where ρ is a reflection coefficient of the mirror, ε_r stands for the relative permittivity of medium and σ represents the conductivity of mirrors.
Coupling losses α_c can be enumerated from the reflection on the dielectric foil in the following way:

$$\alpha_c = |\rho|^2 = \left[\frac{t}{\lambda}\pi\sqrt{2}\left(\varepsilon_r - 1\right)\right]^2 \quad . \tag{19}$$

Unfortunately, when taking into account the real condition, the theoretical equation of the coupling losses (19) (Engstova, 1973) does not correspond to the results gained from the simulations (more details are discussed in Chapter 2.4.3).
The quality factors for particular losses can be approximated by

$$Q_x = \frac{2\pi d}{\lambda\,\alpha_x} \quad . \tag{20}$$

The total unloaded quality factor can be derived from particular loss components as

$$\frac{1}{Q_0} = \frac{1}{Q_D} + \frac{1}{Q_R} + \frac{1}{Q_c} = \frac{\lambda}{2\pi d}\left(\alpha_D + \alpha_R + \alpha_c\right) . \tag{21}$$

2.4 Numerical modeling

Various models of Fabry-Perot resonator, with different feeding and coupling components, have been investigated (see the example in Fig. 1). Series of numerical principles with respect to the used approximation of the Method of Moments (MLFMM or hybrid technique of MLFMM and UTD) were applied in order to find a workable and efficient model in the numerical simulator FEKO (FEKO website). The differences of applied principles are based on the surface or the volume definition of dielectric parts. The completely workable model (without using any limitations) is based on the surface equivalence principle in line with the used Multi Level Fast Multipole Method.

There are several possibilities how to model the dielectric structures in FEKO. If the surface current method is employed, the surface of the dielectric solid is subdivided into triangles. On the contrary, in case that the volume current method is utilized, the dielectric solid is subdivided into cuboids.

In the first approach, the surface of dielectric parts is subdivided into a surface mesh using triangular elements. Merely the MLFMM method is applied here. In case of the second class of models, the dielectric volume is subdivided into cuboidal elements. The MLFMM+UDT hybrid technique is used here. In fact, the MLFMM method is required due to the electrically large metallic mirrors.

2.4.1 Surface equivalence principle

In general, the Method of Moments utilizes the surface equivalence principle for modeling of dielectric bodies. In this method, the interfaces between different homogeneous regions are subdivided into a surface mesh using the triangular elements. Basic functions are applied to these elements for the equivalent electric and the equivalent magnetic surface currents. Boundary conditions result from the use of equivalent sources.

The dielectric parts of the Fabry-Perot resonator subdivided into the surface mesh using the triangular elements are depicted in Fig. 4a).

The FEKO simulator provides a possibility of simplification of the thin dielectric coupling foil by the employment of the skin effect, where the body of the foil is defined only in one face.

2.4.2 Volume equivalence principle

The Method of Moments can also be applied with the volume equivalence principle. In this case, the volume is subdivided into cuboidal elements. In principle, the polarization current inside the volume element is unknown. Nevertheless, the volume element has usually more unknowns than a surface mesh, which represents one of drawbacks of this approach. However, this technique is highly suitable for thin sheets and proves to be very stable for low frequencies. Therefore the coupling dielectric foil as a thin structure was modeled by utilization of this technique.

The subdivision of the dielectric parts of the Fabry-Perot resonator into cuboidal elements can be seen in Fig. 4b). Unfortunately, it was observed that particularly at higher frequencies

the lens consisting of cuboidal elements results in an unstable process of the MLFMM+UTD hybrid method. The MLFMM+UDT method introduces a suitable tool for thin structures (equal or less than the wavelength), but not for thick structures (such as the dielectric lens).

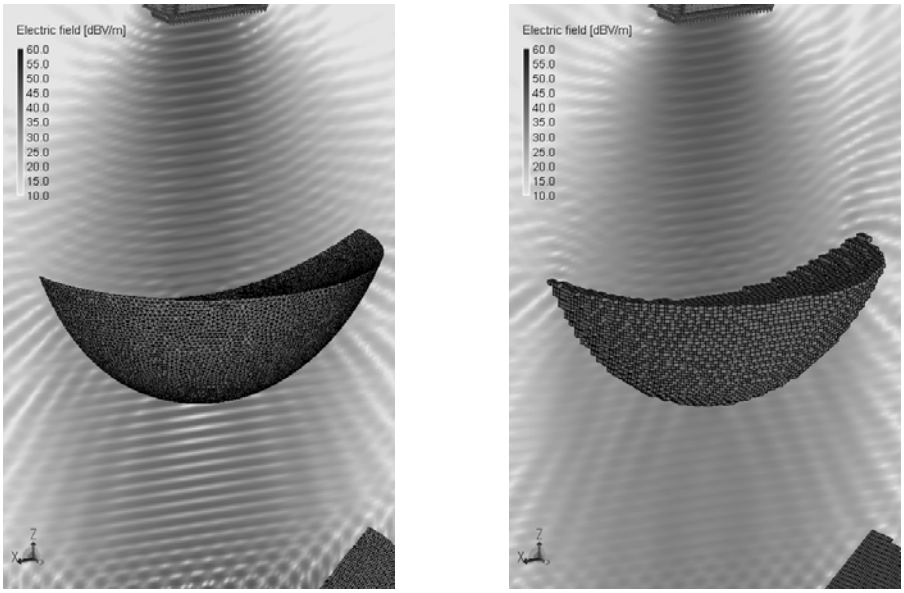

a) b)

Fig. 4. Dielectric parts subdivided by a) surface equivalence principle into triangular elements or by b) volume equivalence principle into cuboidal elements

As a result, the simplified model consisting of the spherical mirrors and dielectric coupling foil was created. The dielectric lens was not considered and the volume equivalence principle was used on the dielectric coupling foil. As for the source, the ideal point source with $\cos^{24}$ radiation pattern (corresponding to the antenna gain of 20 dBi) was used here instead of the actual source of the horn antenna. The main virtue of the proposed approach is the fact that this model can be used particularly at higher frequencies (up to 110 GHz), with respect to computational requirements.

2.4.3 Influence of dielectric coupling foil

The influence of the polyethylene coupling foil (ε_r = 2.26) was investigated from the numerical simulations via the simplified model described above. Frequency dependences of the quality factor under effect of coupling losses and the coupling coefficient are indicated for three different thicknesses of the polyethylene coupling foil; see Fig. 5.

It is necessary to point out that the impact of the dielectric foil on the measurement sensitivity (with regards to the quality factor) is considerably frequency-dependent. The influence of the dielectric foil on the coupling loss can be explained by a smaller depth of penetration at a lower working frequency. This causes low coupling, where reflection

aspects only cannot be involved in the coupling enumeration at lower frequencies. Indeed, also other phenomena have to be taken into account.

The quality factor Q_c, derived from simulation results (Q_0), decreases at lower frequencies due to the low coupling; see Fig. 5a). The values of Q_c were evaluated from (21). The increased reflection of electromagnetic waves can be observed at higher frequencies; therefore losses rise in accordance with (19). It is necessary to emphasize that the obtained effect of the dielectric coupling foil approaches the theoretical definition (19) only at higher frequencies of the coupling foil usability.

The thickness of the coupling foil has to be carefully selected, i.e. it is necessary to take into account the low coupling losses and optimal coupling coefficient (κ within the interval from 0.5 to 2) and set it in harmony with the above-mentioned factors. In our particular case (Fig. 5) the optimal thickness of the foil equals 0.1 mm.

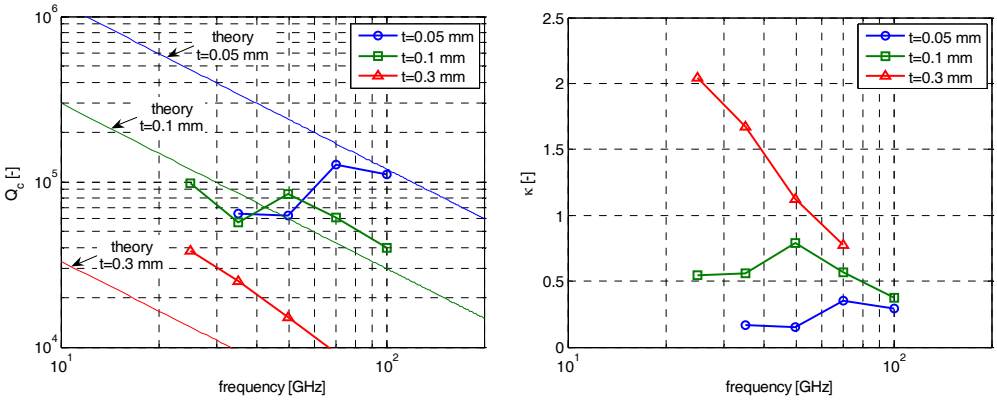

a) b)

Fig. 5. Frequency dependence of a) quality factor under effect of coupling losses and b) coupling coefficient for three different thicknesses of polyethylene coupling foil

2.4.4 Higher-order modes

Since it is necessary to develop a resonator for a wide frequency band, i.e. the Fresnel number N ranges from 1 to higher numbers (note N=1 at the lowest frequency usability of the stable resonator), the emergence of higher-order modes is inevitable. Simulations were performed in order to validate the higher-order modes of the resonator. It was determined that in case of the mirror distance higher than radii of the curvature of mirrors, the higher even modes $TEM_{10,20}$ of the Fabry-Perot resonator are shifted towards higher frequencies. Fig. 6 depicts the particular analyzed frequency distribution of modes for the non-confocal resonator deployment (the distance between mirrors is of 0.493 m, radii of curvatures equals 0.455 m and radii of mirrors amounts to 0.075 m) around the frequency of 110 GHz (corresponds to q=361 and N=4.18). As in our practice case, the source input power of 10 dBm was chosen.

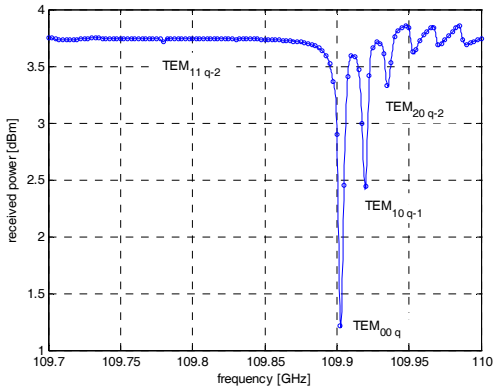

Fig. 6. Higher-order modes around frequency of 110 GHz

The principle of the electric field distribution in transverse plane is demonstrated for instance in (Grabow, 1996) and (Kogelnik, 1966). A longitudinal distribution of the electric field intensity of distinguishable TEM modes inside the resonator is shown in Fig. 7. The maximum energy of the dominant mode TEM_{00} is accumulated in the axis of the resonator. Since the majority of measurements are performed at the dominant mode, it is essential to properly adjust the Gaussian mode shape so that as much active molecules of measured gas as possible are affected by the homogeneous electromagnetic field.

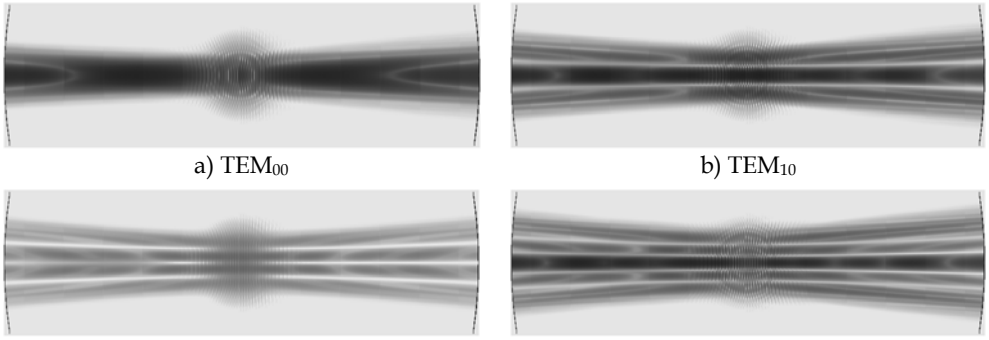

a) TEM_{00} b) TEM_{10}

c) TEM_{11} d) TEM_{20}

Fig. 7. Electric field distribution along resonator at resonant frequencies of particular TEM_{plq} modes

It was derived from the measurements and simulations that the turn of the coupling foil essentially influences the odd transverse mode TEM_{11}. This phenomenon could be almost neglected by a proper setting of the foil and mirrors. On the contrary, an improper setting of the coupling foil could result even in the attenuation at this mode (which would be comparable with the dominant mode). This phenomenon would worsen the identification of operating frequencies. It could be stressed that the mode TEM_{11} lies approximately in the middle of two dominant modes.

2.4.4 Full model

In order to comprehend the other influences (caused by an actual source and by the reflections) in analyses, the full model was developed. The latter comprises the whole system including two spherical mirrors, dielectric coupling foil, two dielectric lenses and actual source of horn antenna. The horn antenna was substituted by its simulated near-field in order to utilize the MLFMM method. The arrangement of particular parts of the resonator was indicated in Fig. 1. The model employs the surface equivalence principle.

In the above-mentioned simplified model with the ideal point sources, the resonator was excited by a spherical wave. Contrary to that, in the full model with dielectric lenses, the resonator is excited by a plane wave. This approach enables a better excitation of the dominant TEM_{00} mode inside the resonator. A better insight into the quality factor of the resonator can be then obtained from simulations - without the degradation of results by an imperfect source.

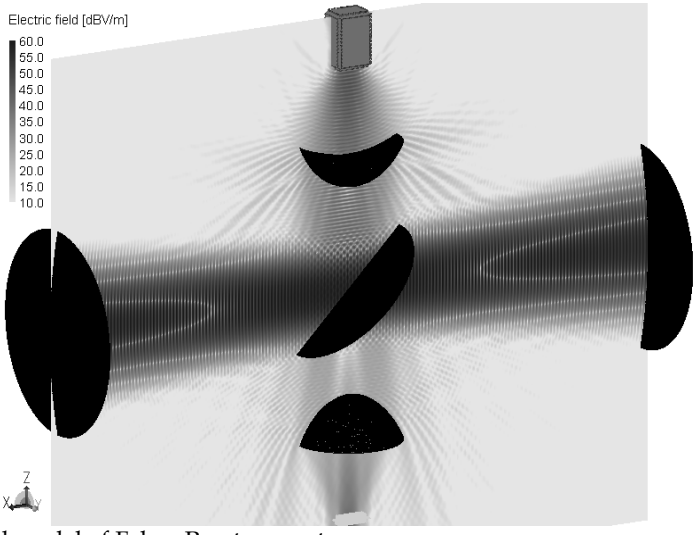

Fig. 8. The full model of Fabry-Perot resonator

The quality factors of $0.8 \cdot 10^5$ and $1.1 \cdot 10^5$ can be determined from simulations performed for both the simplified model and the full model (see Fig. 8), respectively. A particular resonator configuration in this case equaled R=0.455 m, d=0.495-0.510 m, a=0.075 m and frequency usability 26-80 GHz – it corresponds to N within the interval ranging from 1 to 3.

The response of the modeled resonator is described by the frequency dependence of the transmission coefficient. This resonance curve is demonstrated in Fig. 9. From the resonance curve, the unloaded quality factor as well as the coupling coefficient was enumerated in accordance with the process mentioned at the end of Chapter 2.2.

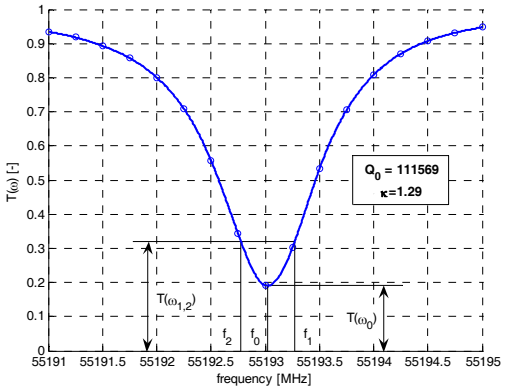

Fig. 9. Resonance curve of modeled resonator

2.5 Methodology of resonator design

From the solution of ABCD matrix of the resonator (indeed under the condition of keeping the beam inside the resonator) the resonator dimensions have to fulfill the following stability condition, which constitutes the first limitation:

$$0 < g_1 \, g_2 < 1 \ . \tag{22}$$

This can be expressed graphically as stable and unstable areas; see Fig. 10.

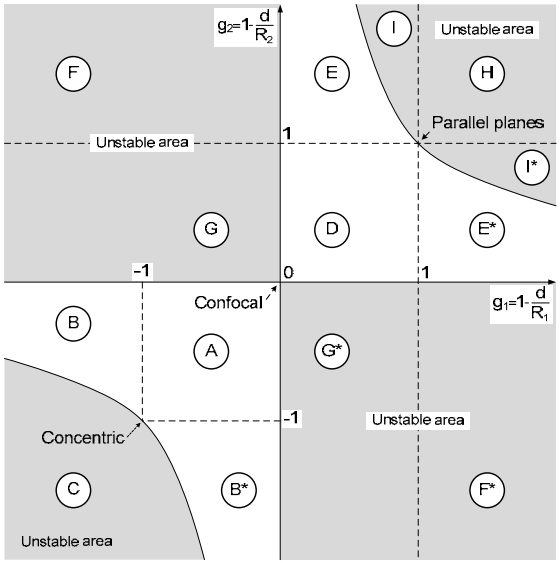

Case	Arrangement	Stability
A		Stable
B, B*		Stable
C		Unstable
D		Stable
E, E*		Stable
F, F*		Unstable
G,G*		Unstable
H		Unstable
I, I*		Unstable

Fig. 10. Stability diagram of open resonators

The second limitation takes into account the diffraction losses. In principle, the diffraction losses of the dominant mode TEM_{00} can be neglected by using the curved reflectors and the correct plate separation d (when Fresnel number N=1). N is given by

$$N = \frac{a_1 a_2}{\lambda d} \ . \tag{23}$$

The arrangement of mirrors is usually set as a near-confocal in order to avoid an overlap of modes TEM_{00} and TEM_{10}. Higher-order modes are the cause of the high Fresnel number, where these higher-order modes show lower diffraction losses.
The excitation of the resonator has a crucial impact on the rise in higher-order modes as well. The ideal source (as a plane wave that incidents perpendicularly to the resonator cavity) creates a pure excitation of the dominant TEM_{00} mode.

3. Millimeter-wave gas absorption measurement

The main advantage of gas absorption laboratory measurements is represented by the fact that the measured medium can be accurately adjusted in terms of the homogeneity of a particular gas composition and distribution, which cannot be truly described in case of open measurements. The high sensitivity of the Fabry-Perot resonant cavity results from its very high quality factor.

3.1 Attenuation constant

The propagation constant γ is defined by

$$\gamma = \alpha + \mathrm{j}\beta = \pm\sqrt{\Gamma^2 - \omega^2 \mu\varepsilon} \ , \tag{24}$$

where α is the attenuation constant in $Np \cdot m^{-1}$, and β stands for the phase constant stated in radians per meter, Γ represents the transverse propagation constant, ω describes the angular frequency, μ is the permeability, while ε stands for the complex permittivity of the medium given by

$$\varepsilon = \varepsilon'(1 - \mathrm{j}\ \mathrm{tg}\ \delta) \ . \tag{25}$$

By taken equation (25) into (24), as well as by the separation of real and imaginary parts and, furthermore, by solving these equations we get the complex relations for α and β (Tysl & Ruzicka, 1989, p. 67).
In case of the low-loss medium (loss factor tg δ << 1) and neglecting of Γ, the attenuation constant can be determined as

$$\alpha = \frac{\pi}{\lambda} \mathrm{tg}\ \delta \ . \tag{26}$$

The medium influences the quality factor in accordance with

$$\frac{1}{Q_0'} = \frac{1}{Q_0} + \mathrm{tg}\ \delta \ . \tag{27}$$

The quality factor Q_0 and the coupling coefficient κ can be obtained from the measurement without gas by means of the approach described in Chapter 2.2.
Very narrow spectral lines can deform the resonance curve of the resonator and also the resulting gas-filled quality factor Q_0'. Therefore, the loss factor can be expressed more accurately with the help of the relation to the coupling coefficient fulfilling (6), which can be obtained from the measurement of the transmission coefficient merely at the resonant frequency by (12). The loss factor can be then expressed from the coupling coefficients without (κ) and with the sample gas (κ') as follows.

$$\text{tg}\,\delta = \frac{1}{Q_0}\left(\frac{\kappa}{\kappa'} - 1\right). \tag{28}$$

By taken equation (28) into (26), the attenuation constant can be given by

$$\alpha = \frac{\pi}{\lambda Q_0}\left(\frac{\kappa}{\kappa'} - 1\right) \quad \text{(Np/m)} \tag{29}$$

or

$$\alpha = \frac{27.288}{\lambda Q_0}\left(\frac{\kappa}{\kappa'} - 1\right) \quad \text{(dB/m)}. \tag{30}$$

We can find these final equations e.g. in (Valkenburg & Derr, 1966).
Parameters of the theoretical equation (11) of resonance curve were optimized by means of the measured data of CH_3CN. The example of the fitting around the resonant frequency of 55193 MHz is depicted in Fig. 11.

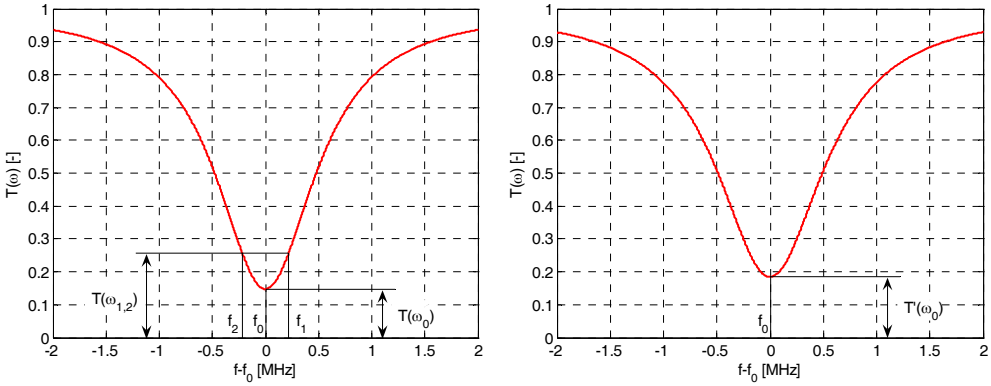

Fig. 11. Fitted measured resonance curves of a) empty and b) gas (CH_3CN)- filled resonator

3.2 Measurement

The measuring system fully controlled by the computer was developed in the Department of electromagnetic field, Czech Technical University in Prague (see setup illustrated in Fig. 12). It involves mixers and multipliers working within the band ranging from 50 to 110 GHz.

By means of the automated step-motor the adjustment of the cavity length from 0.495 to 0.510 m with a 0.05 μm step can be accomplished.

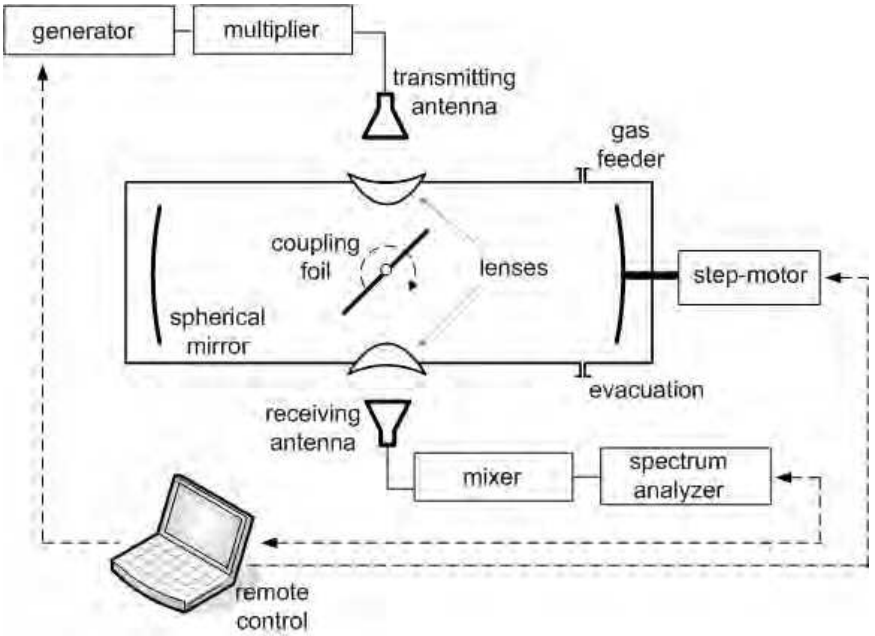

Fig. 12. Fabry-Perot resonator setup for gas absorption measurements (Zvanovec et al., 2009)

First, the received power was measured when the resonator was not coupled. Second, by turning of the coupling foil the resonator was coupled to the minimum received power at the resonance frequency. The transmission coefficient was determined by the received power with the coupling divided by the received power without coupling. The frequency dependence of the transmission coefficient describes the resonance curve. In next step, the resonator was retuned with the adjusting of mirrors distance by a step-motor and the resonance curve was measured again. The process of measurement of resonance curves was repeated also for the case of the gas-filled resonator. From the measured resonance curves, the unloaded quality factor and the coupling coefficient of the empty as well as gas-filled resonator were enumerated in accordance with the process mentioned at the end of Chapter 2.2.
In order to clearly demonstrate the measurement approach, the examples of measured results for the gas of acetonitrile CH_3CN are shown in Fig. 13 and Fig. 14. The curves in Fig. 13 illustrate frequency dependences of the unloaded quality factor and coupling coefficients of the empty and gas-filled resonator. It is obvious that the unloaded quality factor remains stable around the value of 128 000.

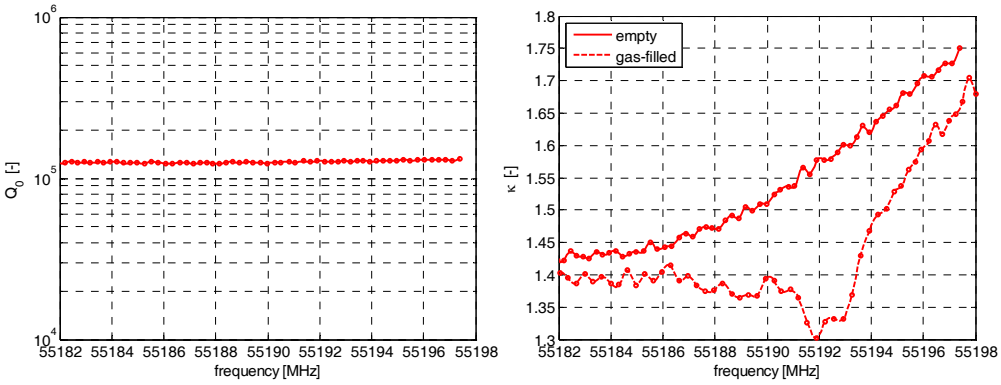

a) b)

Fig. 13. Measured a) unloaded quality factor and b) coupling coefficient with and without gas

The gas absorption loss (attenuation constant) was enumerated from the unloaded quality factor and the coupling coefficients with the help of (30). The frequency dependence of the gas absorption loss is depicted in Fig. 14.

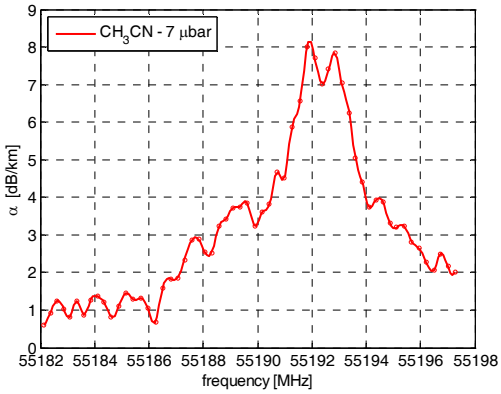

Fig. 14. Gas absorption loss of acetonitrile CH_3CN under pressure of 7 μbar

4. Conclusions

In this chapter, specific millimeter-wave features of the Fabry-Perot resonator were discussed. The main contents include the proposal for fundamental steps (based on the theoretical knowledge and simulations analyses) crucial for the design of the resonator for spectroscopic measurements. The electrically large structures are very complicated to be simulated because of the computational requirement. Hence, the approximation methods were selected. The Multi Level Fast Multipole Method and the Uniform Theory of Diffraction approximation of Method of Moments were tested. As a result, the full model was proposed.

Owing to the simulation in FEKO and the analysis in MATLAB, the electromagnetic field going through the resonator and its analyzed frequency dependence of power (which represents the simulated resonance curve) were obtained. Firstly, parameters of the Fabry-Perot resonator, such as the unloaded quality factor and the coupling coefficient, were evaluated from the simulated resonance curve. Secondly, the theoretical resonance curve is solved by application of latter parameters into the theoretical equation (11). Finally, it is necessary to point out that there is a very good agreement between the theoretical and simulated resonance curves.

The high sensitivity of the Fabry-Perot resonant cavity results from its very high quality factor. The quality factor is reduced with the losses inside the resonator, where the coupling losses caused by the dielectric coupling foil are crucial. Hence, the numerical simulations of the influence of the coupling foil were performed. In our practical case, we qualified the frequency usability of the resonator.

The Fabry-Perot resonator represents a tool for millimeter-wave spectroscopic measurements and fine measurement of medium loss for a propagation purpose. In case that the gas CH_3CN was measured, the measuring procedure was verified. A satisfactory agreement of the unloaded quality factor of the empty resonator between the simulation (Q_0=1.1·10^5) and the measurement (Q_0=1.3·10^5) was achieved. The coupling coefficient turned out to be more sensitive, which is obvious from the comparison of the results for the simulation (κ=1.29) with those relating to the measurement (κ=1.6).

The entire approach concerning the theoretical simulation and practical analyses considerably extends the comprehension of particular millimeter-wave phenomena.

It is necessary to sum up the following important results. The overall resonator was modeled using approximation of the Method of Moments. The thickness of the dielectric coupling foil can be determined for the optimal coupling in advance in order to perform the measurement in the requested frequency band. On the other hand, the dielectric foil shows a considerable, highly frequency-dependent, influence on the resonator parameters, such as quality factor and coupling coefficient. Moreover, the coupling coefficient of the resonator varies with the resonator retuning. The aforementioned effect increases the system measurement error. As a goal for our future research work, we plan to strive to decrease these negative effects and increase the system sensitivity.

5. Acknowledgments

We would like to express our gratitude to Professor Václav Tysl for his experienced advice in the field of the theoretical background on the Fabry-Perot resonator. The work was supported through grants obtained from the Czech Science Foundation (GACR 102/08/P346) and from the Ministry of Education, Youth and Sports of the Czech Republic (research programs LC06071 and MSM 6840770014).

6. References

Montgomery, C. G. (1947). *Technique of Microwave Measurements,* McGraw-Hill

French, I. P., Arnold, T. E. (1967). High-Q Fabry-Perot Resonator for Nitric Oxide Absorption Measurements at 150 GHz. *Review of Scientific Instruments,* Vol. 38, 1967, pp. 1604-1607

Zimmerer, R. W. (1963). Spherical Mirror Fabry-Perot Resonators. *IEEE MTT*, Vol. 11, No. 5, Sept. 1963, pp. 371-379, ISSN 0018-9480

Hirvonen, T. M., Vainikainen, P., Lozowski, A., Räisänen, V. (1996). Measurement of Dielectrics at 100 GHz with an Open Resonator Connected to a Network Analyzer. *IEEE MTT*, Vol. 45, No. 4, Aug. 1996, pp. 780-786

Grabow, J.-U. (2009). *Frontiers of Molecular Spectroscopy,* chap. 14: Microwave Spectroscopy: Experimental Techniques. Elsevier, p. 383-454, ISBN 978-0-444-53175-9

Grabow, J.-U. (1996). A multioctave coaxially oriented beam-resonator arrangement Fourier-transform microwave spectrometer. *Review of Scientific Instruments,* Vol. 67, Dec. 1996, pp. 4072-4084

Chew, W. C., Jin, J.-M., Michielssen, E., Song, J. (2001). *Fast and Efficient Algorithms in Computational Electromagnetics*. Artech, ISBN 1-58053-152-0.

Milligan, T. A. (2005). *Modern Antenna Design, 2nd ed*. Wiley, ISBN 978-0-471-45776-3

Johnson, R. C. (1993). *Antenna Engineering Handbook, third ed*. McGraw-Hill, ISBN 0-07-032381-X

Fox, A. G., Li, T. (1961). Resonant modes in a maser interferometer. *Bell Sys. Tech. J.*, Vol. 40, March 1961, pp. 453-488

Kogelnik, H., Li T. (1966). Laser Beams and Resonators. *Proceedings of the IEEE*, Vol. 54, No. 10, Oct. 1966, pp. 1312-1329

Tysl, V., Ruzicka, V. (1989). *Teoretické základy mikrovlnné techniky*. SNTL, Prague, ISBN 80-03-00141-2 (in czech)

Engstova, R. (1973). *Fabry-Perotův rezonátor pro mikrovlnnou spektroskopii plynu*. Disertation thesis, CTU FEE, Prague, Dec. 1973 (in czech)

Valkenburg, E. P., Derr, V. E. (1966). A High-Q Fabry-Perot Interferometer for Water Vapor Absorption Measurements in the 100 Gc/s to 300 Gc/s Frequency Range. *Proceedings of the IEEE*, Vol. 54, No. 4, April 1966, pp. 493-498

Arora, R. K., Mongia, R. K. (1992). Simple expressions for diffraction loss in open resonators. *Microwave Opt. Tech. Lett.*, vol. 5, August 1992, pp. 401-403

Zvanovec, S., Cerny, P., Piksa, P., Korinek, T., Pechac, P., Mazanek, M., Varga, J., Koubek, J., Urban, S. (2009). The use of the Fabry–Perot interferometer for high resolution microwave spectroscopy. *J. Mol. Spectrosc.*, Vol. 256, No. 1, July 2009, pp. 141–145, ISSN 0022-2852

FEKO website. Available: http://www.feko.info

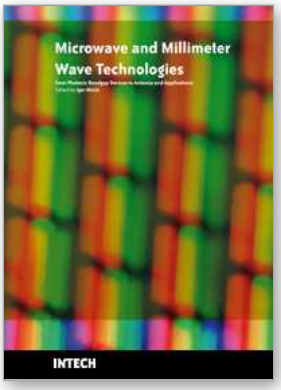

Microwave and Millimeter Wave Technologies from Photonic Bandgap Devices to Antenna and Applications

Edited by Igor Minin

ISBN 978-953-7619-66-4
Hard cover, 468 pages
Publisher InTech
Published online 01, March, 2010
Published in print edition March, 2010

The book deals with modern developments in microwave and millimeter wave technologies, presenting a wide selection of different topics within this interesting area. From a description of the evolution of technological processes for the design of passive functions in milimetre-wave frequency range, to different applications and different materials evaluation, the book offers an extensive view of the current trends in the field. Hopefully the book will attract more interest in microwave and millimeter wave technologies and simulate new ideas on this fascinating subject.

How to reference

In order to correctly reference this scholarly work, feel free to copy and paste the following:

Petr Piksa, Stanislav Zvanovec and Petr Cerny (2010). Specific Millimeter-Wave Features of Fabry-Perot Resonator for Spectroscopic Measurements, Microwave and Millimeter Wave Technologies from Photonic Bandgap Devices to Antenna and Applications, Igor Minin (Ed.), ISBN: 978-953-7619-66-4, InTech, Available from: http://www.intechopen.com/books/microwave-and-millimeter-wave-technologies-from-photonic-bandgap-devices-to-antenna-and-applications/specific-millimeter-wave-features-of-fabry-perot-resonator-for-spectroscopic-measurements

INTECH
open science | open minds

InTech Europe
University Campus STeP Ri
Slavka Krautzeka 83/A
51000 Rijeka, Croatia
Phone: +385 (51) 770 447
Fax: +385 (51) 686 166
www.intechopen.com

InTech China
Unit 405, Office Block, Hotel Equatorial Shanghai
No.65, Yan An Road (West), Shanghai, 200040, China
中国上海市延安西路65号上海国际贵都大饭店办公楼405单元
Phone: +86-21-62489820
Fax: +86-21-62489821